International Journal of Mathematics Trends and Technology
ISSN: 2231-5373/ https://doi.org/10.14445/22315373/IJMTT-V72I1P112

Volume 72 Issue 1, 167-185, January 2026

Original Article

Study of the *N*-Soliton Solutions of the (2+1)-Dimensional Nonlinear Wave Equation

Wuming Li[1], Geyao Li[2]

[1,2]*School of Mathematics and Information Science, Henan Polytechnic University, Jiaozuo, China.*

[1]*Corresponding Author : liwum0626@126.com*

Received: 28 November 2025 Revised: 04 January 2026 Accepted: 22 January 2026 Published: 31 January 2026

Abstract - *In this paper, a (2+1)-dimensional nonlinear wave equation is investigated using the Hirota bilinear method. The N-soliton solutions of this Equation are constructed, and the corresponding local characteristics are analyzed. By selecting specific parameters, various localized waves are derived, including kink solitons, lump solitons, periodic solitons, and so on. Furthermore, the dynamical behaviors of the soliton solutions are exhibited by using the symbolic computation system Maple, and the interaction characteristics of these solutions are elaborated through the corresponding images. Lastly, the ansatz approach is utilized to work out an interesting inelastic interaction solution where lump solitons can occur. These findings in this study are very helpful for deepening the comprehension of the interaction mechanisms exhibited by localized waves in nonlinear wave equations.*

Keywords - *Nonlinear Wave Equation, Hirota Bilinear Method, Soliton Solution, Lump Solution, Periodic Solution.*

1. Introduction

Solitons are an important research subject in integrable systems, and they have wide applications in various fields, such as plasma physics, optical fibers, fluid mechanics, oceanic shock waves, molecular systems, and Bose-Einstein condensates [1–5]. Therefore, to obtain the soliton solutions of nonlinear partial differential equations, various methods for finding exact solutions have been constructed, including the inverse scattering transformation [6–7], The Bäcklund Transformation [8–9], The Darboux Transformation [10–11], The Riemann-Hilbert Approach [12–13], The Sine-Gordon Expansion Approach [14], The Modified Kudryashov Approach [15–16], The Hirota Bilinear Method [17–18], and Other Approaches [19]. For the above-mentioned methods, each has its own merits. However, to the best of our knowledge, no single method can solve all known nonlinear equations so far.

In 1971, the Hirota bilinear method was introduced for directly solving nonlinear wave equations [20]. Owing to the simplicity and effectiveness of this method, it has been widely employed to obtain *N*-soliton solutions for various nonlinear partial differential equations. Over the past decades, this approach has played an important role in integrable systems [21]. In [22], the lump solution of the Burgers equation is derived using the bilinear method, and the author further studies its interaction solutions. [23] investigated the lump solutions of many types of partial differential equations via the Hirota bilinear formulation. [17] systematically studied the (2+1)-dimensional generalized Hirota-Satsuma-Ito equation using the Hirota bilinear method and obtained various localized soliton solutions. Motivated by the aforementioned works, this paper investigates a (2+1)-dimensional nonlinear wave equation [22] using the Hirota bilinear method, which is written as

$$u_{xt} + \alpha_1(u_{xyyy} - 3u_y u_{yy} - 3w_y u_{xy}) + \alpha_2 u_{xx} + \alpha_3 u_{yy} = 0, u_y = w_x. \quad (1)$$

where$u = u(x, y, t)$ serves as the potential function representing the amplitude distribution of solitons, where x and y denote the soliton's propagation directions in the two-dimensional spatial plane, and t represents the temporal variable. The parametersα_1,α_2,$\alpha_3$are physical constants that characterize the key properties of the solitons, including dispersion strength, nonlinear modulation intensity, and transverse wave propagation speed. By tuning these parameters to different values, this Equation can vividly describe a diverse range of intriguing nonlinear phenomena in shallow water systems, such as the formation of multi-soliton interactions, the propagation of lump waves, and the modulation instability of wave trains. Therefore, in this work, we conduct a systematic and in-depth investigation into the *N*-soliton solutions of this Equation using the Hirota bilinear method, which allows us to derive exact analytical expressions for solitons and reveal their dynamic evolution behaviors. Furthermore, we present the interaction solutions between solitons and other localized wave structures, and most notably, we successfully construct the lump solution via the ansatz method—a result that not only enriches the solution family of the Equation but also provides a theoretical basis for understanding the non-oscillatory, localized wave phenomena observed in shallow water environments.

In the existing literature, numerous scholars have carried out in-depth research on relevant nonlinear wave equations from multiple perspectives. For instance, [24] focused on the Painlevé integrability of a (2+1)-dimensional nonlinear wave equation, and successfully derived its multi-soliton, breather, and lump solutions through rigorous theoretical deductions. [25] investigated an extended form of a generalized (2+1)-dimensional bilinear equation, and explored its integrability characteristics comprehensively from various angles, providing a solid theoretical basis for subsequent studies. By employing the bilinear method, [26] obtained a variety of soliton solutions for the nonlinear wave equation, and further derived *M*-lump solitons by virtue of the long wave limit transformation, enriching the solution forms of such equations. [27] Conducted a systematic investigation on a (2+1)-dimensional nonlinear wave equation based on the Hirota bilinear method; in addition, by applying the asymptotic analysis technique with two-soliton parameter constraints, the authors successfully obtained *X*-type and *Y*-type solitons, which expanded the understanding of soliton interaction behaviors.

Although the Hirota bilinear method has been maturely applied to solving soliton solutions, existing studies still have limitations. Most of them only focus on the construction of soliton solutions, with insufficient quantitative analysis on the parameter selection of the bilinear form and dynamic characteristics such as soliton collision behavior. Aiming at the above limitations, this study establishes a quantitative analysis framework for the correlation between bilinear parameters and dynamic characteristics. Combining numerical simulation with theoretical derivation, it clarifies the influence of the coefficient parameters in the bilinear Equation on soliton collision, thus enriching the application of the Hirota bilinear method in the analysis of nonlinear systems.

Therefore, different from the above-mentioned works, the core goal of this study is to put forward an efficient approach to constructing novel categories of soliton solutions for Equation (1) by leveraging the Hirota bilinear method. Specifically, the *N*-soliton solutions of this Equation are first derived and their intrinsic local properties analyzed. Furthermore, the evolutionary behaviors of interactions between various soliton solutions are graphically exhibited via Maple software. The subsequent structure of this paper is arranged as follows: In Section 2, the *N*-soliton solutions of the Equation are derived, and then various types of localized wave interaction solutions are obtained by constraining and assigning values to the parameters of the soliton solutions. Section 3 focuses on presenting the inelastic interaction solutions of mixed lump-kink solitons for Equation (1) and conducts a visual discussion on the inelastic interactions between these soliton solutions. Finally, this research is summarized in Section 4.

2. The *N*-Soliton Solution of the (2+1)-Dimensional Nonlinear Wave Equation

In this section, the Hirota bilinear method is used to obtain the *N*-soliton solution of Equation (1). In order to transform the nonlinear Equation (1) into a bilinear form, the following Hopf-Cole transformation is performed

$$u = -2(\ln f)_x,\ w = -2(\ln f)_y \tag{2}$$

For Equation (1), integrating with respect to x once and setting the integration constant to 0, we obtain

$$2(\ln f)_{xt} + \alpha_1(2(\ln f)_{xyyy} + 3(2(\ln f)_{xy} \cdot (2(\ln f)_{yy}))) + \alpha_2(2(\ln f)_{xx} + \alpha_3(2(\ln f)_{yy} = 0 \tag{3}$$

The bilinear form of Eq.(1) is as follows

$$(D_t D_x + \alpha_1 D_x D_y^3 + \alpha_2 D_x^2 + \alpha_3 D_y^2) f \cdot f = 0 \tag{4}$$

whereD_t,$D_x$and$D_y$are bilinear derivative operators, defined as

$$D_x^l D_y^n D_t^m f \cdot g = (\partial_x - \partial_{x'})^l (\partial_y - \partial_{y'})^n (\partial_t - \partial_{t'})^m f(x,y,t) g(x',y',t') | x = x', y = y', t = t' \tag{5}$$

The Eq.(4) is equivalent to

$$f f_{xt} - f_x f_t + \alpha_1(f_{xyyy} f - 3 f_{xyy} f_y + 3 f_{xy} f_{yy} - f_x f_{yyy}) + \alpha_2(f f_{xx} - f_x^2) + \alpha_3(f f_{yy} - f_y^2) = 0 \tag{6}$$

Here, the function f is assumed to have the following form, expressed as

$$f = 1 + \sum_{N}^{i=1} e^{\eta_i} + \sum_{N}^{i<j} A_{ij} e^{\eta_i + \eta_j} + \sum_{N}^{i<j<k} A_{ij} A_{ik} A_{jk} e^{\eta_i + \eta_j + \eta_k} + \cdots + (\prod_{i<j} A_{ij}) e^{\sum_{N}^{i=1} \eta_i} \tag{7}$$

where

$$\eta_i = a_i x + b_i y + c_i t + \eta_{0i}, c_i = -\frac{\alpha_1 a_i b_i^3 + \alpha_2 a_i^2 + \alpha_3 b_i^2}{a_i} \tag{8}$$

$$A_{ij} = -\frac{\alpha_1 (a_i - a_j)(b_i - b_j)^3 + \alpha_2 (a_i - a_j)^2 + \alpha_3 (b_i - b_j)^2 + (a_i - a_j)(c_i - c_j)}{\alpha_1 (a_i + a_j)(b_i + b_j)^3 + \alpha_2 (a_i + a_j)^2 + \alpha_3 (b_i + b_j)^2 + (a_i + a_j)(c_i + c_j)}\ i, j = 1,2, \cdots, N \tag{9}$$

Moreover, the parametersa_i,$b_i$and$\eta_{0i}$are constants.

2.1. The One-Soliton Solution

To derive the one-soliton solution of Equation (1), by virtue of Equation (7), we have the following expression

$$f = 1 + e^{\eta_1} \tag{10}$$

The one-soliton solution to Equation (1), which is derived by substituting Equation (10) into the bilinear transformation in Equation (2), is given as

$$u = -a_1[1 + tanh(\frac{\eta_1}{2})] \tag{11}$$

$$w = -b_1[1 + tanh(\frac{\eta_1}{2})] \tag{12}$$

where$\eta_1 = a_1 x + b_1 y + c_1 t + \eta_{01}$.

Specifically, taking the parameters$a_1 = 1, b_1 = -1, \eta_{01} = 0, \alpha_1 = 1, \alpha_2 = -1, \alpha_3 = -1$in Equations (11) and (12), we can obtain the specific expressions of *u* and *w*. It is noticed that setting$a_1 = 1$leads to negative values for the component *u*, while setting $b_1 = -1$ results in positive values for the component *w*. With the parameters$\alpha_1 = 1, \alpha_2 = -1, \alpha_3 = -1$ and $t = 0$, we acquire the one-soliton solution to Equation (1), with the corresponding 3D structural plot and 2D density plot presented in Figure 1. As visualized in the figure, the *u* and *w* exhibit characteristics of a kink soliton and an anti-kink soliton, respectively.

2.2. The Two-Soliton Solutions

In this subsection, a study is conducted on the classification and value assignment of the parameters of the two-soliton solution under four different scenarios, thereby obtaining soliton types with distinct morphologies. A detailed analysis of these cases is presented below. When$N = 2$it follows from Equation (7) that

$$f = 1 + e^{\eta_1} + e^{\eta_2} + A_{12} e^{\eta_1 + \eta_2} \tag{13}$$

The two-soliton solution of Equation (1) is obtained by substituting Equation (13) into Equation (2). The expressions for yo*u* and *w* are

$$u = -2\frac{a_1 e^{\eta_1} + a_2 e^{\eta_2} + A_{12}(a_1 + a_1) e^{\eta_1 + \eta_2}}{1 + e^{\eta_1} + e^{\eta_2} + A_{12} e^{\eta_1 + \eta_2}} \tag{14}$$

$$w = -2\frac{b_1 e^{\eta_1} + b_2 e^{\eta_2} + A_{12}(b_1 + b_1) e^{\eta_1 + \eta_2}}{1 + e^{\eta_1} + e^{\eta_2} + A_{12} e^{\eta_1 + \eta_2}} \tag{15}$$

where$\eta_1 = a_1 x + b_1 y + c_1 t + \eta_{01}, \eta_2 = a_2 x + b_2 y + c_2 t + \eta_{02}$.

2.2.1. The Two-Kink Soliton Solutions

When all parameters take real values, two kink-shaped soliton solutions are derived, with the specific cases detailed as follows. Specifically, taking the parameters $a_1 = 3, b_1 = 2, a_2 = 5, b_2 = 7, \eta_{01} = 0, \eta_{02} = 0, \alpha_1 = 4, \alpha_2 = 2, \alpha_3 = 1,$ the two-soliton solutions are obtained, and the corresponding structures are shown in Figure 2. Specifically, Figure 2 (a1),(b1) displays the two kink soliton structures of solution *u*, while Figures 2 (a2),(b2) illustrate the two kink soliton structures of solution *w*. From the density plots, it can be observed that the kink solution of yo*u* exhibits an *X*-shape in the plane, whereas the kink solution of *w* exhibits a *Y*-shape.

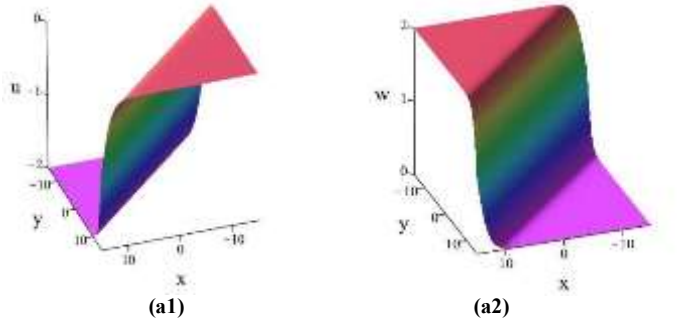

(a1) **(a2)**

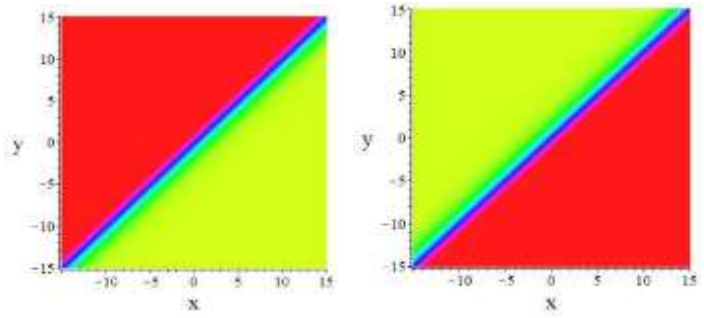

(b1) (b2)

Fig. 1 The One-Soliton Solution of the Equation (1) at $t = 0$; (a1) 3D Structure of u;(a2) 3D Structure of w; (b1) 2D Density Plot of u; (b2) 2D Density Plot of w

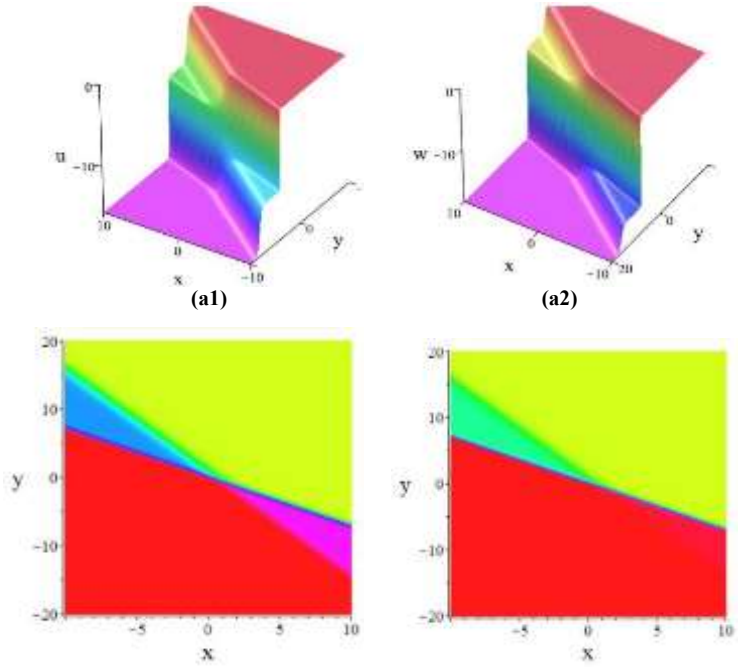

(a1) (a2)

(b1) (b2)

Fig. 2 The Two-Soliton Solution of the Equation (1) at $t = 0$; (a1) 3D Structure of u; (a2) 3D Structure of w; (b1) 2D Density Plot of u; (b2) 2D Density Plot of w

2.2.2. One y-Periodic Soliton Solutions

A notable phenomenon emerges when transitioning from Section 2.2.1 to Section 2.2.2, namely that the periodic solutions arise as parameter values change from real to imaginary numbers. Specifically, taking the parameters $a_1 = 1, b_1 = i, a_2 = 2, b_2 = -i, \eta_{01} = 0, \eta_{02} = 0, \alpha_1 = 4, \quad \alpha_2 = 3, \alpha_3 = 5, t = 0$, where i is the imaginary unit satisfying $i^2 = -1$, the soliton structures of yo$u$ and w are shown in Figure 3. As observed from Figure 3, when b_1 and b_2 take purely imaginary values, the profile of the two-soliton solution transforms from a kink solution to a localized breathing solution, with both u and w being perpendicular to the x-axis.

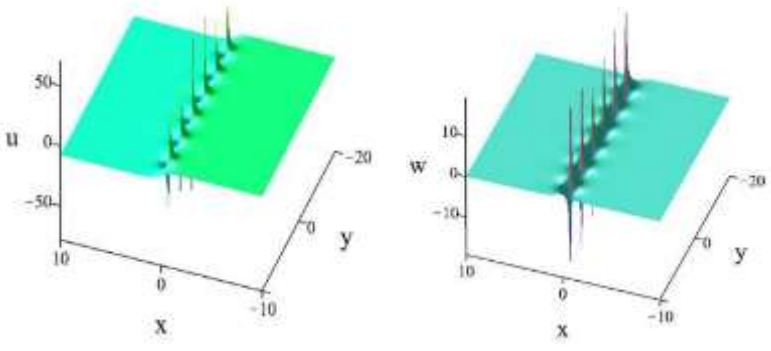

(a1) (a2)

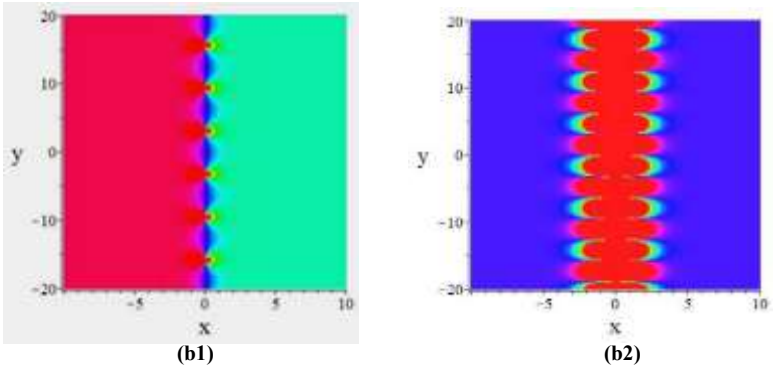

(b1) (b2)

Fig. 3 The *y*-Periodic Soliton Solution of the Equation (1) at $t = 0$; (a1) 3D Structure of *u*; (a2) 3D Structure of *w*; (b1) 2D Density Plot of *u*; (b2) 2D Density Plot of *w*

2.2.3. One (x, y)-Periodic Soliton Solutions

When some of the parameters vary from purely imaginary values to complex numbers, the periodic solutions of Equation (1) trans- form from *y*-type to (*x,y*)-type. Specifically, taking the parameters$a_1 = 1, b_1 = 1 + i, a_2 = 2, b_2 = 1 - i, \eta_{01} = 0, \eta_{02} = 0, \alpha_1 = -0.1, \alpha_2 = 3, \alpha_3 = 5,$ the solutions *u* and *w* with (*x, y*)-periodic soliton structures $t = 0$are shown in Figure 4.

When b_1 and b_2 take complex values, the periodic solitons are no longer oriented perpendicularly to the *x*-axis, with their movement shifting toward the *y*-direction. In the course of a collision, the solution retains its shape with merely a phase offset generated, a key property inherent to soliton solutions.

2.2.4. One Lump Soliton Solutions

The lump solitons are remarkable due to their unique stability and localization. Under the condition of some small parameters, their energy distribution and density profiles exhibit sharp, well-defined boundaries and concentrated amplitude regions.

We set$a_1 = l_1 \cdot \varepsilon, a_2 = l_2 \cdot \varepsilon, b_1 = n_1 \cdot \varepsilon, b_2 = n_2 \cdot \varepsilon, \eta_{01} = i \cdot \pi, \eta_{02} = -i \cdot \pi,$ into Equation (13). By taking$\varepsilon \to 0$and following the long-wave limit method [29], the function *f* can be expanded into

$$f = \theta_1\theta_2\varepsilon^2 + o(\varepsilon^2) \tag{16}$$

where

$$\theta_1 = l_1x + n_1y - (\alpha_2 l_1 + \frac{\alpha_3 n_1^2}{l_1})t$$

$$\theta_2 = l_2x + n_2y - (\alpha_2 l_2 + \frac{\alpha_3 n_2^2}{l_2})t \tag{17}$$

The lump soliton solutions associated with *u* and *w* can be calculated by substituting Equations (16) and (17) into Equation (3), and their specific forms are illustrated as

$$u = -2(\frac{l_1}{\theta_1} + \frac{l_2}{\theta_2})$$

$$w = -2(\frac{n_1}{\theta_1} + \frac{n_2}{\theta_2}) \tag{18}$$

Specifically, taking the parameter$a_1 = 0.01, b_1 = 0.01 + 0.01i, a_2 = 0.01, b_2 = 0.01 - 0.01i, \eta_{01} = i\pi, \eta_{02} = -i\pi, \alpha_1 = -0.1, \alpha_2 = 3, \alpha_3 = 5,$ we can analyze the lump soliton behavior (as shown in Fig.5). The observed differences in extrema between *u* and *w* may arise from distinct nonlinear dynamics or coupling effects in the underlying Equation, highlighting the richness of soliton behavior in multidimensional systems. Such localized structures have profound implications in various fields such as optical fiber communication, condensed matter physics, quantum technology, and even biological systems.

Table 1 records the classification of different wave types in the soliton solutions of Equation (1) and presents the results of different parameter selections for the two-soliton solution.

Table 1. Types of Two-Soliton Localized Waves for Equation (1) Under Different Parameter Selections

N-soliton solutions	Wave structures	Parameter selections
N=2	Two kink-type solitons	$a_1 = 3, b_1 = 2, a_2 = 5, b_2 = 7, \eta_{01} = 0,$ $\eta_{02} = 0, \alpha_1 = 4, \alpha_2 = 2, \alpha_3 = 1$
	One y-periodic soliton	$a_1 = 1, b_1 = i, a_2 = 2, b_2 = -i, \eta_{01} = 0,$ $\eta_{02} = 0, \alpha_1 = -0.1, \alpha_2 = 3, \alpha_3 = 5$
	One (x, y)-periodic soliton	$a_1 = 1, b_1 = 1+i, a_2 = 2, b_2 = 1-i, \eta_{01} = 0,$ $\eta_{02} = 0, \alpha_1 = -0.1, \alpha_2 = 3, \alpha_3 = 5,$
	One lump soliton	$a_1 = 0.01, b_1 = 0.01 + 0.01i, a_2 = 0.01,$ $b_2 = 0.01 - 0.01i, \eta_{01} = i\pi, \eta_{02} = -i\pi,$ $\alpha_1 = -0.1, \alpha_2 = 3, \alpha_3 = 5,$

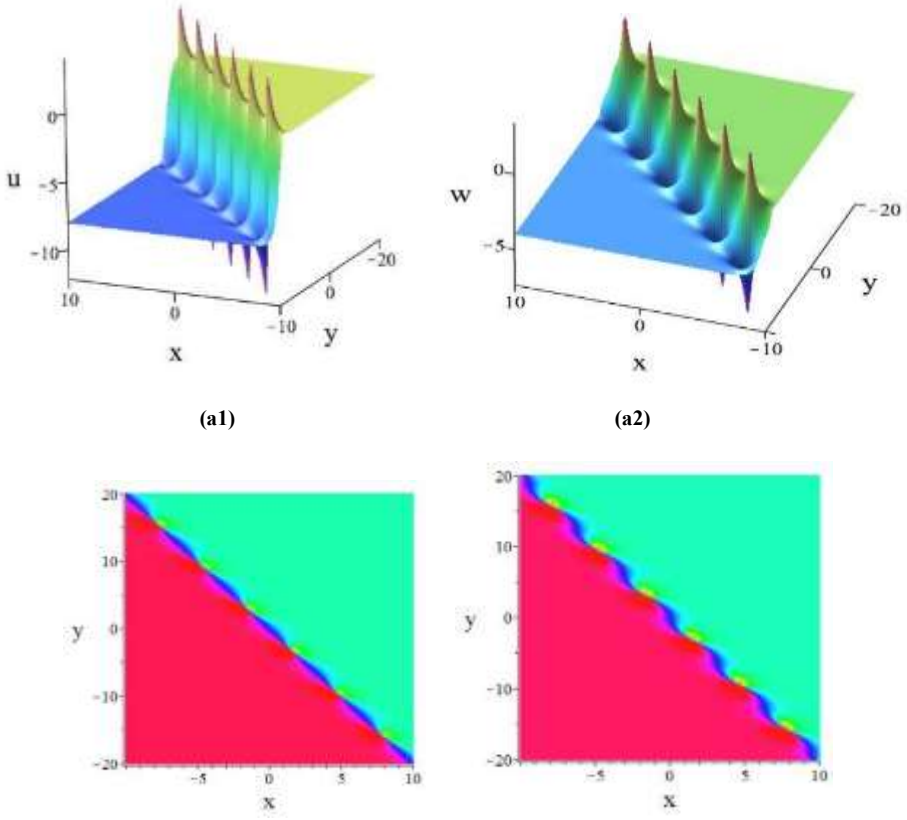

(a1) (a2)

(b1) (b2)

Fig. 4 The (*x*,*y*)-Periodic Soliton Solution of the Equation (1) at *t* = 0; (a1) 3D Structure of *u*; (a2) 3D Structure of *w*; (b1) 2D Density Plot of *u*; (b2) 2D Density Plot of *w*.

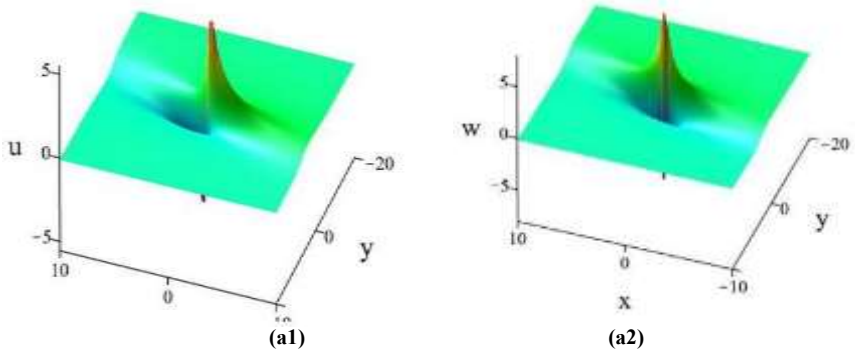

(a1) (a2)

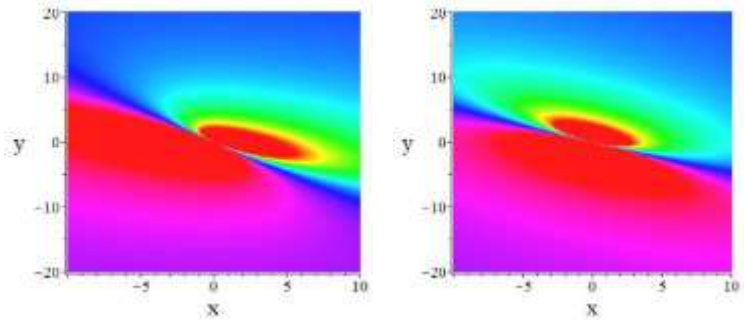

(b1) (b2)

Fig. 5 The Lump Soliton Solution of the Equation (1) at *t* = 0; (a1) 3D Structure of *u*; (a2) 3D Structure of *w*; (b1) 2D Density Plot of *u*; (b2) 2D Density Plot of *w*.

2.3. The Three-Soliton Solutions

In this subsection, four kinds of three-soliton wave solutions are considered. When$N = 3$it follows from Equation (7) that we can obtain

$$f = 1 + e^{\eta_1} + e^{\eta_2} + e^{\eta_3} + A_{12}e^{\eta_1+\eta_2} + A_{13}e^{\eta_1+\eta_3} + A_{23}e^{\eta_2+\eta_3} + A_{123}e^{\eta_1+\eta_2+\eta_3} \tag{19}$$

where $A_{123} = A_{12}A_{13}A_{23}$. The three-soliton solution of Equation (1) is obtained by substituting Equation (19) into Equation (2). Due to the extremely complex forms of the expressions, they are omitted here.

2.3.1. The Three Kink Soliton Solutions

When *N* = 3 and all parameter values are real numbers, Equation (1) yields two kink-type three-soliton solutions *u* and *w*. Specifically, taking the parameters$a_1 = 1, b_1 = 1, a_2 = 1, b_2 = 2, a_3 = 1, b_3 = 3, \eta_{01} = 0, \eta_{02} = 0, \eta_{03} = 0, \alpha_1 = -0.1, \alpha_2 = 0.1, \alpha_3 = 0.1,$ the three-soliton structures $t = 0$are presented in Figure 6. We observe that both *u* and *w* are composed of three kink-shaped solitons.

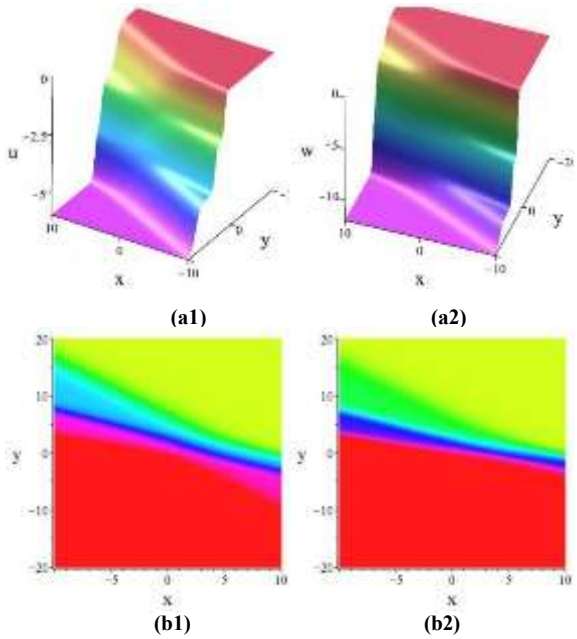

(a1) (a2)

(b1) (b2)

Fig. 6 The three soliton solution of the Eq.(1) at *t* = 0; (a1) 3D structure of *u*; (a2) 3D structure of *w*; (b1) 2D density plot of *u*; (b2) 2D density plot of *w*

2.3.2. One y-Periodic Soliton and One Kink Soliton Solution

When the parameters b_1 and b_2 take purely imaginary values, the three-soliton solution is composed of one *y*-periodic soliton solution and one kink soliton solution. Specifically, the parameters are taken as$a_1 = 1, b_1 = 2i, a_2 = 1, b_2 = -2i, a_3 = 1, b_3 = 0, \eta_{01} = 0, \eta_{02} = 0, \eta_{03} = 0, \alpha_1 = 4,\ \alpha_2 = 2, \alpha_3 = 1.$ Through the utilization of Maple software, we obtain the 3D structures and 2D density plots, which are illustrated in Figures 7 and 8. The parallel interaction between one kink soliton and one *y*-periodic soliton for yo*u* is depicted in Figure 7. As observed, the kink soliton propagates along the positive *x*-axis, while the *y*-periodic soliton propagates along the negative *x*-axis. Before the collision, they propagate at almost the same speed. After interaction, the two parallel solitons move away from each other while retaining their original

shapes and speeds, indicating that their interaction is elastic. Figure 8 shows the parallel movement of the *y*-periodic solitons of *w* over time, with their directions also oriented perpendicularly to the *x*-axis. Furthermore, it is noted that *w* exhibits only a *y*-periodic soliton, propagating along the negative *x*-axis.

2.3.3. One y-Periodic Soliton and One Inclined Kink Soliton Solution

In this subsection, the parameter b_3 is assigned a non-zero value, and the three-soliton solution morphology of Equation (1) manifests a distinct structural shift. Specifically, the parameters $a_1 = 1, b_1 = 2i, a_2 = 1, b_2 = -2i, a_3 = 1, b_3 = 0.5, \eta_{01} = 0, \eta_{02} = 0, \eta_{03} = 0, \alpha_1 = 4, \alpha_2 = 2, \alpha_3 = 1$, are adopted, and the structure of *u* and *w* is derived. The visualization in Figure 9 reveals the interaction between one inclined kink soliton solution and one *y*-periodic soliton solution of yo*u*, and the *y*-periodic soliton is oriented perpendicular to the *x*-axis. Figure 10 depicts the interaction between one inclined kink soliton and one *y*-periodic soliton of *w*. As observed in Figure 10, the kink soliton propagates along the positive *x*-axis while the *y*-periodic soliton propagates along the negative *x*-axis over time. After the interaction, they move away from each other while retaining their original shapes and speeds, indicating that their interaction is elastic.

2.3.4. One Inclined Kink Soliton and One Lump Soliton Solutions

With a_2 and a_3 taking extremely small real values and b_2 and b_3 adopting small conjugate imaginary numbers simultaneously, the solution of Equation (1) exhibits the interaction of one inclined kink soliton and one lump soliton. This interaction not only enriches the soliton solution spectrum of Equation (1) but also provides a new perspective for exploring multidimensional nonlinear dynamics. Specifically, taking the parameters $a_1 = 1, b_1 = 1, a_2 = 0.01, b_2 = 0.01 + 0.01i, a_3 = 0.01, b_3 = 0.01 - 0.01i, \eta_{01} = 0, \eta_{02} = 0, \eta_{03} = 0, \alpha_1 = -1, \alpha_2 = 2, \alpha_3 = 1,$ we can observe the elastic interaction between different types of solitons. The time evolution process of the elastic interaction between the soliton structures of yo*u* is presented in Figure 11. Notably, *w* demonstrates structural similarity to yo*u*, with its interaction dynamics aligning well with those observed for you, as depicted in Figure 12.

Table 2 systematically documents the classification of distinct wave types in the soliton solutions of Equation (1), along with the corresponding parameter tuning strategies for the three-soliton solution used to achieve such classification.

Table 2. Types of Three-Soliton Localized Waves for Equation (1) Under Different Parameter Selections

N-**soliton solutions**	**Wave structures**	**Parameter selections**
N=3	Three kink solitons	$a_1 = 1, b_1 = 1, a_2 = 1, b_2 = 2, a_3 = 1, b_3 = 3, \eta_{01} = 0, \eta_{02} = 0, \eta_{03} = 0, \alpha_1 = -0.1, \alpha_2 = 0.1, \alpha_3 = 0.1.$
	One *y*-periodic soliton and one kink soliton	$a_1 = 1, b_1 = 2i, a_2 = 1, b_2 = -2i, a_3 = 1, b_3 = 0, \eta_{01} = 0, \eta_{02} = 0, \eta_{03} = 0, \alpha_1 = 4, \alpha_2 = 2, \alpha_3 = 1.$
	One *y*-periodic soliton and one inclined kink soliton	$a_1 = 1, b_1 = 2i, a_2 = 1, b_2 = -2i, a_3 = 1, b_3 = 0.5, \eta_{01} = 0, \eta_{02} = 0, \eta_{03} = 0, \alpha_1 = 4, \alpha_2 = 2, \alpha_3 = 1.$
	One lump soliton and one kink soliton	$a_1 = 1, b_1 = 1, a_2 = 0.01, b_2 = 0.01 + 0.01i, a_3 = 0.01, b_3 = 0.01 - 0.01i, \eta_{01} = 0, \eta_{02} = 0, \eta_{03} = 0, \alpha_1 = -1, \alpha_2 = 2, \alpha_3 = 1.$

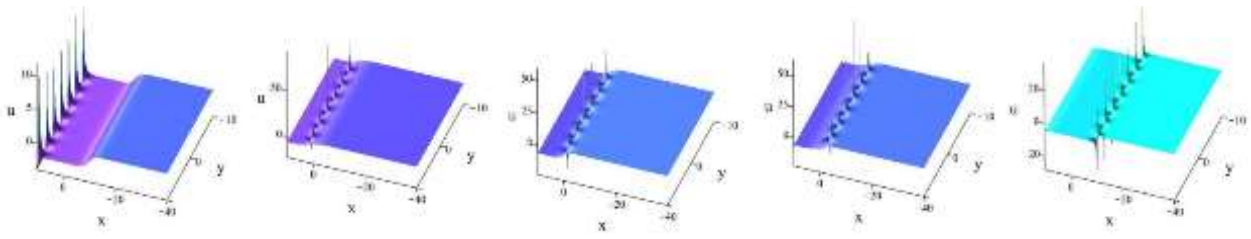

(a1) **(a2)** **(a3)** **(a4)** **(a5)**

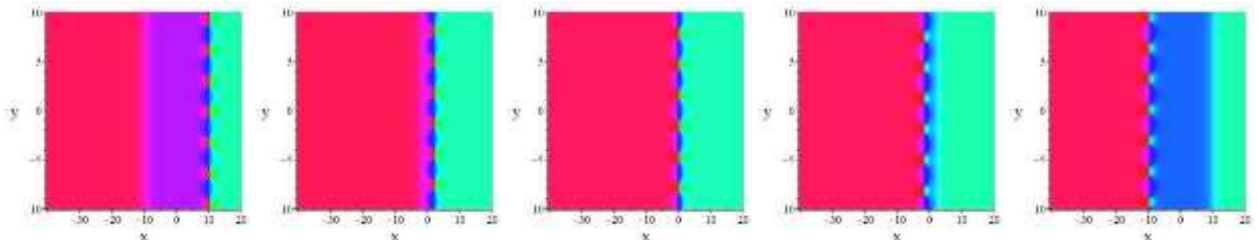

(b1) (b2) (b3) (b4) (b5)

Fig. 7 The Evolution Behavior of the Mixed-Type Soliton of Equation (1) for the component *u*. (a1) 3D Structure at *t* = -5; (a2) 3D Structure at *t* = -1; (a3) 3D Structure at *t* = 0; (a4) 3D Structure at *t* = 1; (a5) 3D Structure at *t* = 5; (b1) 2D Density Plot at *t* = -5; (b2) 2D Density Plot at *t* = -1; (b3) 2D Density Plot at *t* = 0; (b4) 2D Density Plot at *t* = 1; (b5) 2D Density Plot at *t* = 5

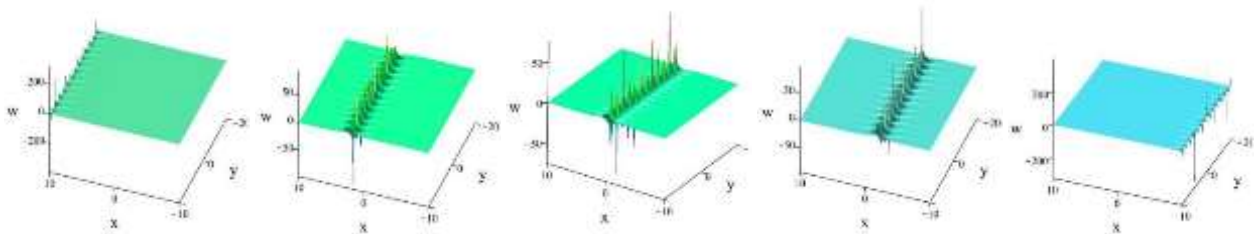

(a1) (a2) (a3) (a4) (a5)

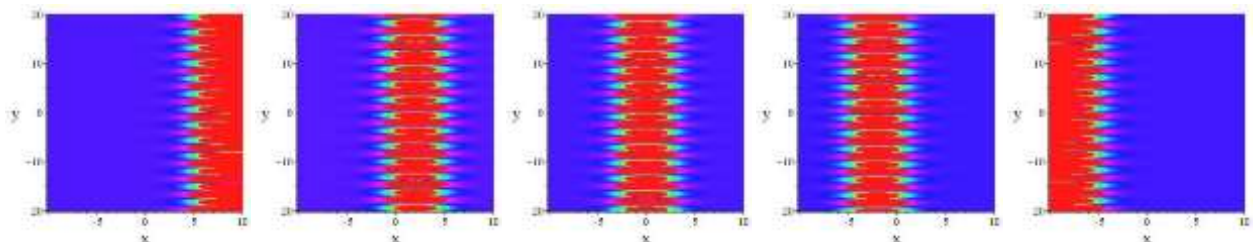

(b1) (b2) (b3) (b4) (b5)

Fig. 8 The Evolution Behavior of the Mixed-Type Soliton of Equation (1) for the component *w*. (a1) 3D Structure at *t* = -5; (a2) 3D Structure at *t* = -1; (a3) 3D Structure at *t* = 0; (a4) 3D Structure at *t* = 1; (a5) 3D Structure at *t* = 5; (b1) 2D Density Plot at *t* = -5; (b2) 2D Density Plot at *t* = -1; (b3) 2D Density Plot at *t* = 0; (b4) 2D Density Plot at *t* = 1; (b5) 2D Density Plot at *t* = 5.

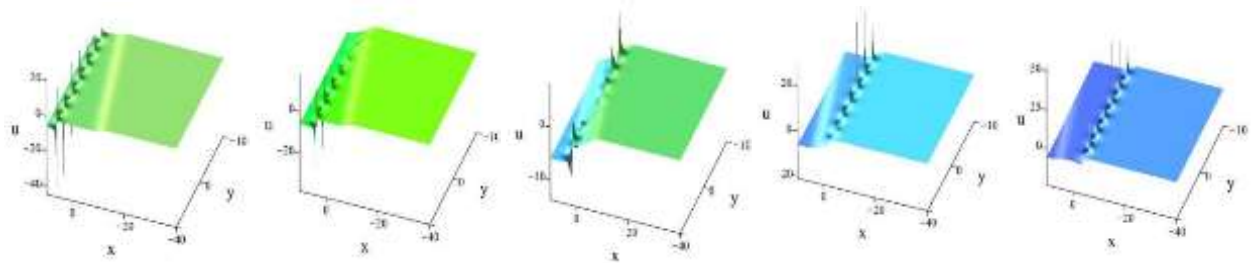

(a1) (a2) (a3) (a4) (a5)

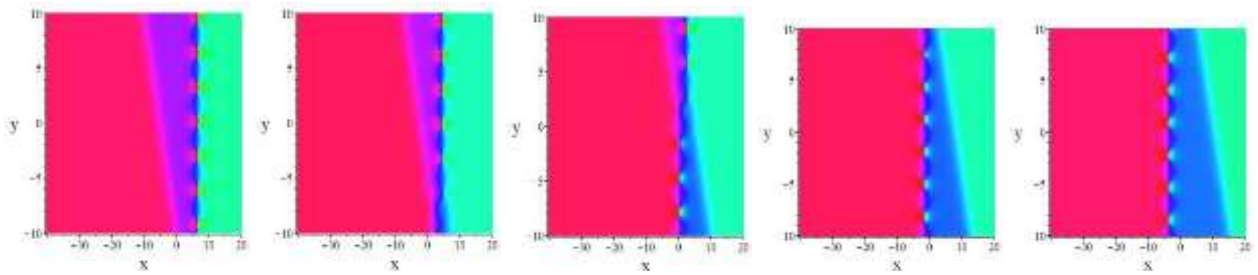

(b1) (b2) (b3) (b4) (b5)

Fig. 9 The Evolution Behavior of the Mixed-Type Soliton of Equation (1) for the component *u*. (a1) 3D Structure at *t* = -3; (a2) 3D Structure at *t* = -1; (a3) 3D Structure at *t* = 0; (a4) 3D Structure at *t* = 1; (a5) 3D Structure at *t* = 3; (b1) 2D Density Plot at *t* = -3; (b2) 2D Density Plot at *t* = -1; (b3) 2D Density Plot at *t* = 0; (b4) 2D Density Plot at *t* = 1; (b5) 2D Density Plot at *t* = 3.

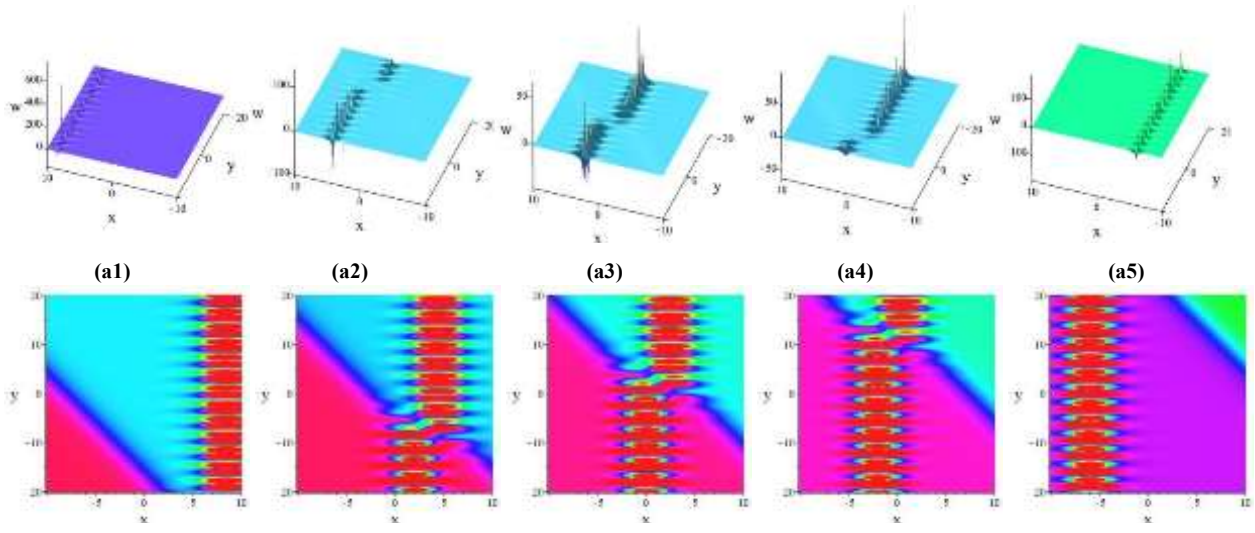

(a1) (a2) (a3) (a4) (a5)

(b1) (b2) (b3) (b4) (b5)

Fig. 10 The Evolution Behavior of the Mixed-Type Soliton of Equation (1) for the component *w*. (a1) 3D Structure at *t* = -3; (a2) 3D Structure at *t* = -1; (a3) 3D Structure at *t* = 0; (a4) 3D Structure at *t* = 1; (a5) 3D Structure at *t* = 3; (b1) 2D Density Plot at *t* = -3; (b2) 2D Density Plot at *t* = -1; (b3) 2D Density Plot at *t* = 0; (b4) 2D Density Plot at *t* = 1; (b5) 2D Density Plot at *t* = 3.

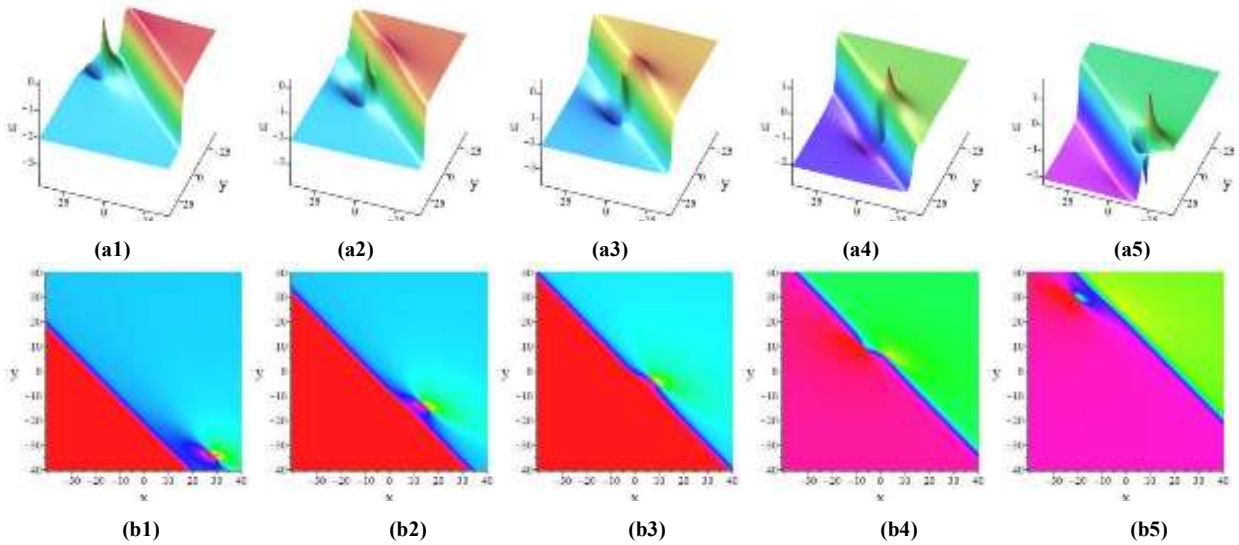

(a1) (a2) (a3) (a4) (a5)

(b1) (b2) (b3) (b4) (b5)

Fig. 11 The Evolution Behavior of the Mixed-Type Soliton of Equation (1) for the component *u*. (a1) 3D Structure at *t* = -3; (a2) 3D Structure at *t* = -1; (a3) 3D Structure at *t* = 0; (a4) 3D Structure at *t* = 1; (a5) 3D Structure at *t* = 3; (b1) 2D Density Plot at *t* = -3; (b2) 2D Density Plot at *t* = -1; (b3) 2D Density Plot at *t* = 0; (b4) 2D Density Plot at *t* = 1; (b5) 2D Density Plot at *t* = 3.

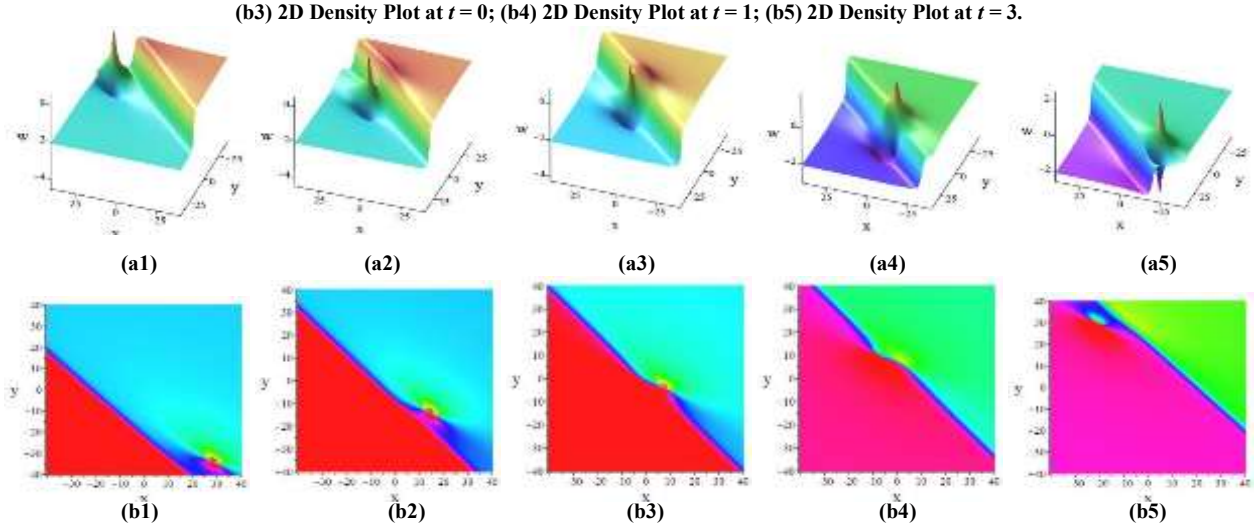

(a1) (a2) (a3) (a4) (a5)

(b1) (b2) (b3) (b4) (b5)

Fig. 12 The Evolution Behavior of the Mixed-Type Soliton of Equation (1) for the Component w. (a1) 3D Structure at t = -3; (a2) 3D Structure at t = -1; (a3) 3D Structure at t = 0; (a4) 3D Structure at t = 1; (a5) 3D Structure at t = 3; (b1) 2D Density Plot at t = -3; (b2) 2D Density Plot at t = -1; (b3) 2D Density Plot at t = 0; (b4) 2D Density Plot at t = 1; (b5) 2D Density Plot at t = 3.

2.4. The Four-Soliton Solutions

Subsequently, we discuss the different cases of the parameter values of Equation (1) from four aspects. When$N = 4$it follows from Equation (7) that we can obtain

$$f = 1 + e^{\eta_1} + e^{\eta_2} + e^{\eta_3} + e^{\eta_4} + A_{12}e^{\eta_1+\eta_2} + A_{13}e^{\eta_1+\eta_3} + A_{14}e^{\eta_1+\eta_4} + A_{23}e^{\eta_2+\eta_3} + A_{24}e^{\eta_2+\eta_4} + A_{34}e^{\eta_3+\eta_4} + A_{123}e^{\eta_1+\eta_2+\eta_3} + A_{124}e^{\eta_1+\eta_2+\eta_4} + A_{134}e^{\eta_1+\eta_3+\eta_4} + A_{234}e^{\eta_2+\eta_3+\eta_4} + A_{1234}e^{\eta_1+\eta_2+\eta_3+\eta_4} \quad (20)$$

Where $A_{1234} = A_{12}A_{13}A_{14}A_{23}A_{24}A_{34}$. The four-soliton solution of Equation (1) is derived by substituting Equation (20) into Equation (2), and its explicit form is omitted here.

2.4.1. The Four Kink Soliton Solutions

When all parameters take real values, the four-kink soliton morphology of Equation (1) is obtained. Specifically, the parameters are taken as $a_1 = 1, b_1 = 1, a_2 = 1, b_2 = 2, a_3 = 1, b_3 = 3, a_4 = 1, b_4 = 4, \eta_{01} = 0, \eta_{02} = 0, \eta_{03} = 0, \eta_{04} = 0, \alpha_1 = -0.1, \alpha_2 = -1, \alpha_3 = -1$, and the four-soliton solutions *u* and *w* of Equation (1) are depicted in Figure 13 at $t = 0$. It is evident that the four-soliton solutions for yo*u* and *w* each correspond to a specific morphology consisting of four kink solitons.

2.4.2. One y-Periodic Soliton and Two Kink Solitons

When b_1 and b_2 take purely imaginary values with $b_4 = 0$, the periodic breather solution and the kink solutions emerge. Specifically, $a_1 = 1, b_1 = 2i, a_2 = 1, b_2 = -2i, a_3 = 1, b_3 = 1, a_4 = 1, b_4 = 0, \eta_{01} = 0, \eta_{02} = 0, \eta_{03} = 0, \eta_{04} = 0, \alpha_1 = 4, \alpha_2 = 3, \alpha_3 = 2$, Figures 14 and 15 present the structural distributions of yo*u* and *w* at various times, respectively. Figure 14 demonstrates the time evolution of the interaction between one *y*-periodic soliton and two kink solitons for yo*u*, which exhibits elastic behavior. Figure 15 shows a similar behavior for *w*, except that the *y*-periodic soliton differs in shape.

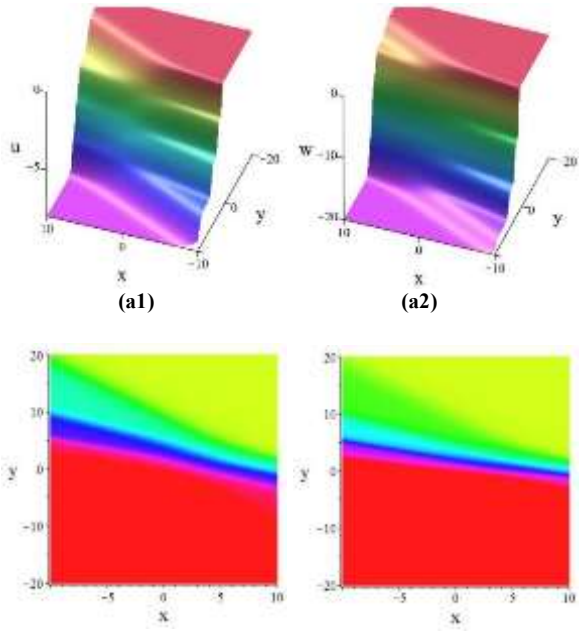

(a1) **(a2)** **(b1)** **(b2)**

Fig. 13 The Four-Soliton Solution of Equation (1) at t = 0; (a1) 3D Structure of u; (a2) 3D Structure of w; (b1) 2D Density Plot of u; (b2) 2D Density Plot of w

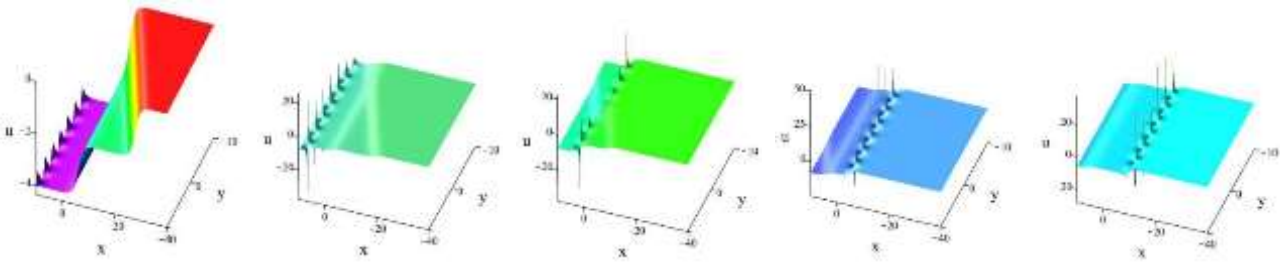

(a1) **(a2)** **(a3)** **(a4)** **(a5)**

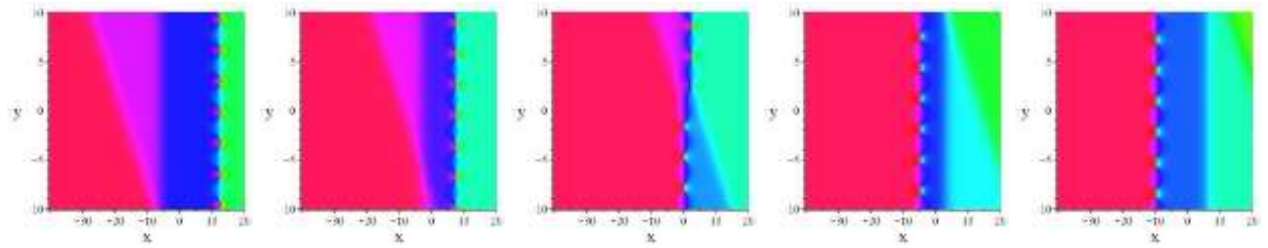

(b1) (b2) (b3) (b4) (b5)

Fig. 14 The Evolution Behavior of the Mixed-Type Soliton of Equation (1) for the Component *u*. (a1) 3D Structure at *t* = -2; (a2) 3D Structure at *t* = -1; (a3) 3D Structure at *t* = 0; (a4) 3D Structure at *t* = 1; (a5) 3D Structure at *t* = 2; (b1) 2D Density Plot at *t* = -2; (b2) 2D Density Plot at *t* = -1; (b3) 2D Density Plot at *t* = 0; (b4) 2D Density Plot at *t* = 1; (b5) 2D Density Plot at *t* = 2.

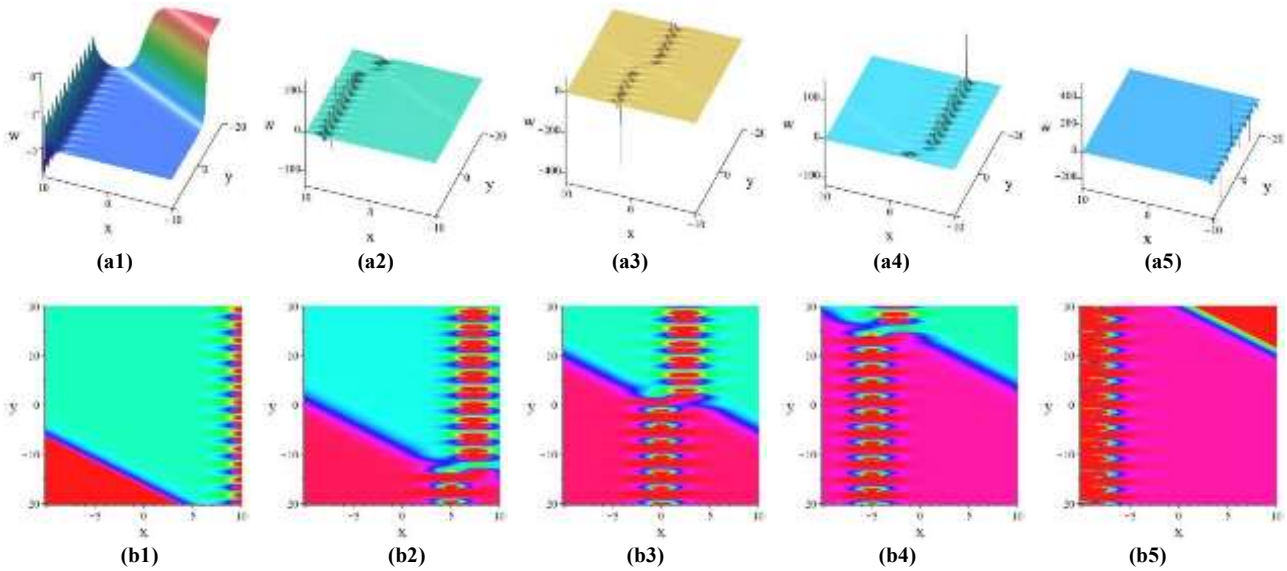

(a1) (a2) (a3) (a4) (a5)

(b1) (b2) (b3) (b4) (b5)

Fig. 15 The Evolution Behavior Of The Mixed-Type Soliton of Equation (1) for the Component *w*. (a1) 3D Structure at *t* = -2; (a2) 3D Structure at *t* = -1; (a3) 3D Structure at *t* = 0; (a4) 3D Structure at *t* = 1; (a5) 3D Structure at *t* = 2; (b1) 2D Density Plot at *t* = -2; (b2) 2D Density Plot at *t* = -1; (b3)2D Density Plot at *t* = 0; (b4) 2D Density Plot at *t* = 1; (b5) 2D Density Plot at $t = 2$.

2.4.3. Two y-Periodic Solitons

When b_1, b_2, b_3, and b_4 all take purely imaginary values, the patterns have changed significantly. Specifically, taking $a_1 = 1, b_1 = i, \quad a_2 = 1, b_2 = -i, a_3 = 1, b_3 = 2i, a_4 = 1, b_4 = -2i, \eta_{01} = 0, \eta_{02} = 0, \eta_{03} = 0, \eta_{04} = 0, \alpha_1 = 4, \alpha_2 = 3, \alpha_3 = 2$, the structural plots pertaining to *u* and *w*, which $t = -2, -1, 0, 1, 2$are illustrated in Figures 16 and 17, respectively. Figure 16 reveals that yo*u* exhibits interactions between two periodic solitons, and its temporal evolution confirms elastic behavior—after collision, the solitons still keep their original form unchanged. Figure 17 shows a similar elastic collision behavior for solution *w*, albeit with distinct periodic soliton morphologies. Remarkably, a distinct fusion and fission process is evident in Figure 17.

2.4.4. One y-Periodic Soliton and One (x, y)-Periodic Soliton

When b_1 and b_2 take purely imaginary values, while b_3 and b_4 take complex values, the soliton structures change noticeably. Specifically, taking the parameters$a_1 = 1, b_1 = i, a_2 = 1, b_2 = -i, a_3 = 1, b_3 = 2 + 2i, a_4 = 1, b_4 = 2 - 2i, \eta_{01} = 0, \eta_{02} = 0, \eta_{03} = 0, \eta_{04} = 0, \alpha_1 = -0.01, \ \alpha_2 = 4, \alpha_3 = 1,$ he structural plots of yo*u* and *w* $t = -2, -1, 0, 1, 2$are depicted in Figures 18 and 19, respectively. Figure 18 shows that the structure of solution *u* consists of one *y*-periodic soliton and one (*x, y*)-periodic soliton. It is noted that as time increases, both solitons propagate toward the positive *x*-axis with continuous interaction, while maintaining their original shapes. Figure 19 shows similar behavior for *w*, albeit with the *y*-periodic soliton propagating toward the positive *x*-axis and the (*x, y*)-periodic soliton toward the positive *y*-axis, while their shapes remain unchanged.

Table 3 summarizes the characteristic types of distinct waves, which are obtained by selecting appropriate parameters for the four-soliton solution of Equation (1).

Table 3 Types of Three-Soliton Localized Waves for Equation (1) Under Different Parameter Selections

N-soliton solutions	Wave structures	Parameter selections
$N = 4$	Four kink solitons	$a_1 = 1, b_1 = 1, a_2 = 1, b_2 = 2, a_3 = 1, b_3 = 3,$ $a_4 = 1, b_4 = 4, \eta_{01} = 0, \eta_{02} = 0, \eta_{03} = 0,$ $\eta_{04} = 0, \alpha_1 = -0.1, \alpha_2 = -1, \alpha_3 = -1.$
	One *y*-periodic soliton and two kink solitons	$a_1 = 1, b_1 = 2i, a_2 = 1, b_2 = -2i, a_3 = 1,$ $b_3 = 1, a_4 = 1, b_4 = 0, \eta_{01} = 0, \eta_{02} = 0,$ $\eta_{04} = 0, \alpha_1 = 4, \alpha_2 = 3, \alpha_3 = 2.$
	Two *y*-periodic solitons	$a_1 = 1, b_1 = i, a_2 = 1, b_2 = -i, a_3 = 1,$ $b_3 = 2i, a_4 = 1, b_4 = -2i, \eta_{01} = 0, \eta_{02} = 0,$ $\eta_{03} = 0, \eta_{04} = 0, \alpha_1 = 4, \alpha_2 = 3, \alpha_3 = 2.$
	One *y*-periodic soliton and one (x, y)-periodic soliton	$a_1 = 1, b_1 = i, a_2 = 1, b_2 = -i, a_3 = 1,$ $b_3 = 2 + 2i, a_4 = 1, b_4 = 2 - 2i,$ $\eta_{01} = 0, \eta_{02} = 0, \eta_{03} = 0, \eta_{04} = 0, \alpha_1 = -0.01, \alpha_2 = 4, \alpha_3 = 1.$

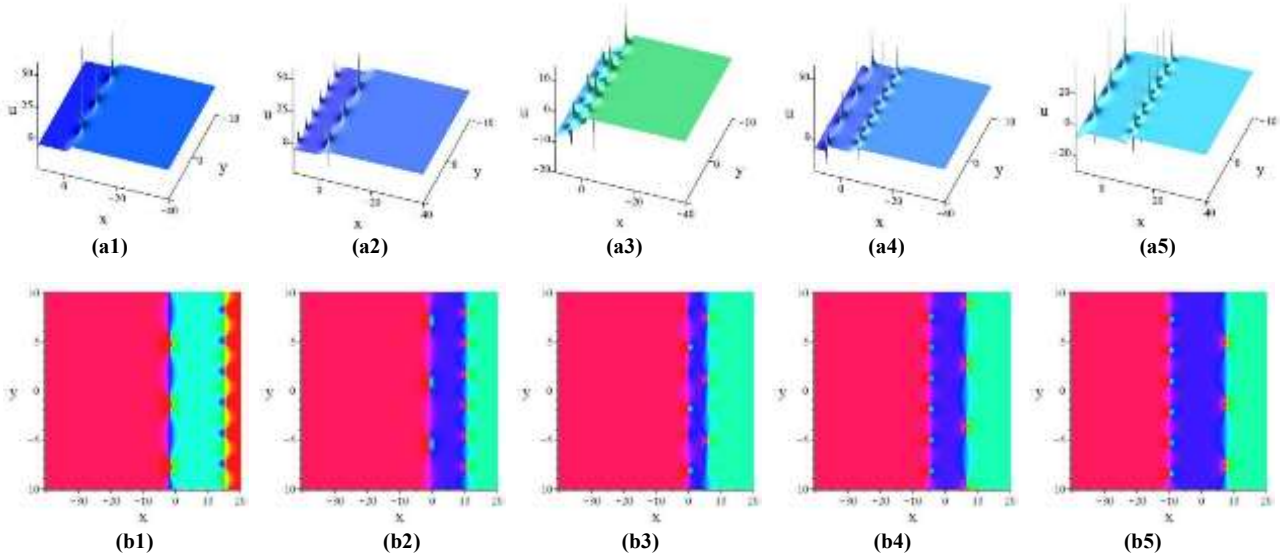

Fig. 16 The Evolution Behavior of the Mixed-Type Soliton of Equation (1) for the Component *u*. (a1) 3D Structure at *t* = -2; (a2) 3D Structure at *t* = -1; (a3) 3D Structure at *t* = 0; (a4) 3D Structure at *t* = 1; (a5) 3D Structure at *t* = 2; (b1) 2D Density Plot at *t* = -2; (b2) 2D Density Plot at *t* = -1; (b3) 2D Density Plot at *t* = 0; (b4) 2D Density Plot at *t* = 1; (b5) 2D Density Plot at *t* = 2.

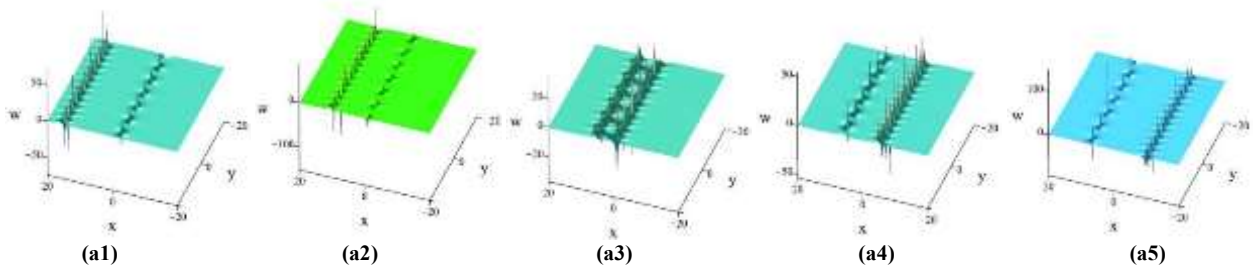

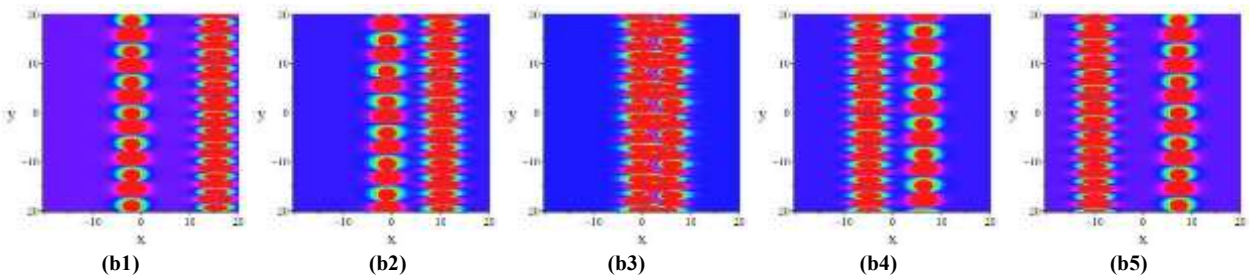

(b1) (b2) (b3) (b4) (b5)

Fig. 17 The Evolution Behavior of the Mixed-Type Soliton of Equation (1) for the Component w. (a1) 3D Structure at t = -2; (a2) 3D Structure at t = -1; (a3) 3D Structure at t = 0; (a4) 3D Structure at t = 1; (a5) 3D Structure at t = 2; (b1) 2D Density Plot at t = -2; (b2) 2D Density Plot at t = -1; (b3) 2D Density Plot at t = 0; (b4) 2D Density Plot at t = 1; (b5) 2D Density Plot at t = 2.

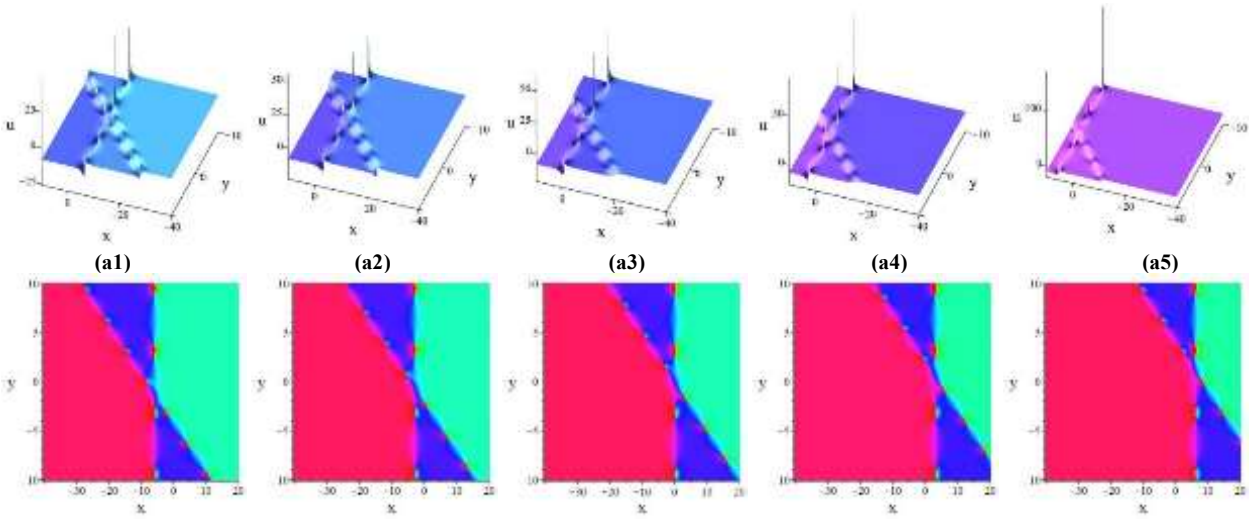

(a1) (a2) (a3) (a4) (a5)

(b1) (b2) (b3) (b4) (b5)

Fig. 18 The Evolution Behavior of the Mixed-Type Soliton of Equation(1) for the Component u. (a1) 3D Structure at t = -2; (a2) 3D Structure at t = -1; (a3) 3D Structure at t = 0; (a4) 3D Structure at t = 1; (a5) 3D Structure at t = 2; (b1) 2D Density Plot at t = -2; (b2) 2D Density Plot at t = -1; (b3) 2D Density Plot at t = 0; (b4) 2D Density Plot at t = 1; (b5) 2D Density Plot at t = 2.

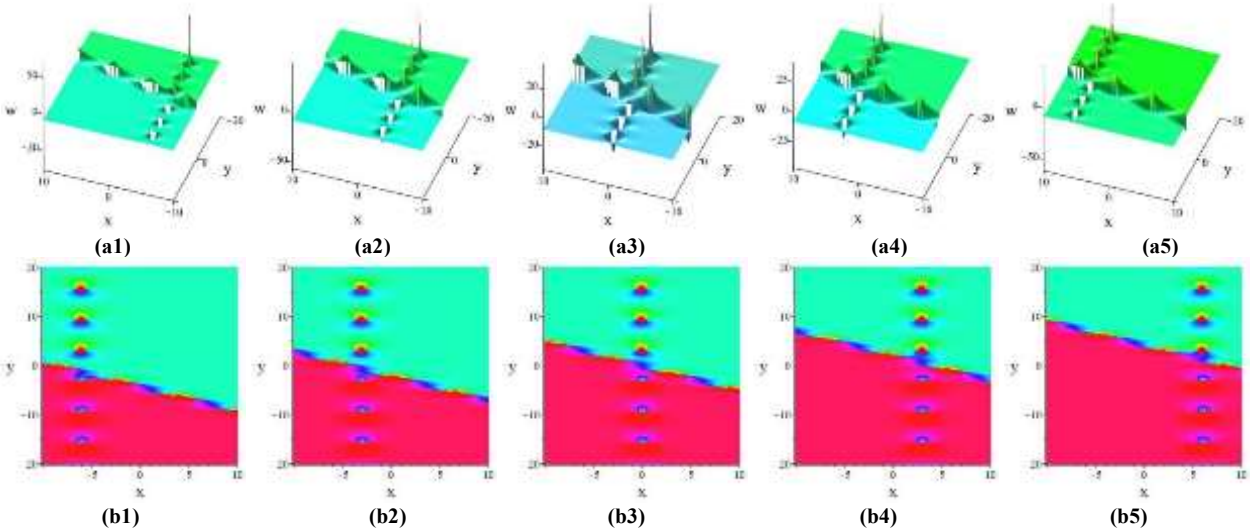

(a1) (a2) (a3) (a4) (a5)

(b1) (b2) (b3) (b4) (b5)

Fig. 19 The Evolution Behavior of the Mixed-Type Soliton of Equation (1) for the Component w. (a1) 3D Structure at t = -2; (a2) 3D Structure at t = -1; (a3) 3D Structure at t = 0; (a4) 3D Structure at t = 1; (a5) 3D Structure at t = 2; (b1) 2D Density Plot at t = -2; (b2) 2D Density Plot at t = -1; (b3) 2D Density Plot at t = 0; (b4) 2D Density Plot at t = 1; (b5) 2D Density Plot at t = 2.

3. The Inelastic Interactions Between Different Types of Solitons

We have examined in detail the various solutions describing elastic interactions for Equation (1) in Section 2. By contrast, within this section, some novel inelastic interaction solutions are derived by using the ansatz method.

The Eq.(1) is equivalent to

$$D_xD_t(f,f)+\alpha_1(D_xD_y^3(f,f)+\alpha_2(D_x^2(f,f))+\alpha_3(D_y^2(f,f)))$$
$$=2(\frac{\partial^2}{\partial t\partial x}f)f-2(\frac{\partial}{\partial x}f)(\frac{\partial}{\partial t}f)+\alpha_1(2(\frac{\partial^4}{\partial x\partial y^3}f)f-6(\frac{\partial^3}{\partial x\partial y^2}f)(\frac{\partial}{\partial y}f)+6(\frac{\partial^2}{\partial x\partial y}f)(\frac{\partial^2}{\partial y^2}f)$$
$$-2(\frac{\partial}{\partial x}f)(\frac{\partial^3}{\partial y^3}f))+\alpha_2(2(\frac{\partial^2}{\partial x^2}f)f-2(\frac{\partial}{\partial x}f)^2)+\alpha_3(2(\frac{\partial^2}{\partial y^2}f)f-2(\frac{\partial}{\partial y}f)^2) \quad (21)$$

To achieve this end, it is set that

$$f=g^2+h^2+ke^l \quad (22)$$

with

$$g=a_1x+a_2y+a_3t+a_4$$
$$h=a_5x+a_6y+a_7t+a_8$$
$$l=k_1x+k_2y+k_3t+k_4 \quad (23)$$

where$a_i(1\le i\le 8)$, k and$k_j(1\le j\le 4)$ are undetermined parameters. After substituting Equations (22) and (23) into Equation (6), all terms are collected with the same power of$x^iy^jt^k\,exp(l)^m$, where$i,j,k,m\in Z$, and set their coefficients to zero to solve the Equation, thereby deriving an overdetermined system of nonlinear algebraic equations for the unknown$a_i$and$k_j(i=1,2,\cdots,8;j=1,2,\cdots,4)$.

Using the symbolic computation software Maple, we can solve for the values of $a_i$andk_j. Here, we present one set of results as follows

$$k=k,k_1=-\frac{2\alpha_3}{3\alpha_1k_2},k_2=k_2,k_3=\frac{3\alpha_1^2k_2^4+4\alpha_2\alpha_3}{6\alpha_1k_2},k_4=k_4,$$
$$a_1=\frac{2\alpha_3\alpha_6}{3\alpha_1k_2^2},a_2=-\frac{3a_5k_2^2\alpha_1}{2\alpha_3},a_3=\frac{(9\alpha_1^2k_2^4-4\alpha_2\alpha_3)a_6}{6\alpha_1k_2^2},$$
$$a_4=a_4,a_5=a_5,a_6=a_6,a_7=\frac{(9\alpha_1^2k_2^4-4\alpha_2\alpha_3)a_5}{4\alpha_3},a_8=a_8 \quad (24)$$

Substituting Equation (24) into Equation (22) and (23) and setting $k>0$, the expression for *f* can be obtained, which is written as

$$f=(t\cdot\frac{(9\alpha_1^2k_2^4-4\alpha_2\alpha_3)a_6}{6\alpha_1k_2^2}+\frac{2x\alpha_3a_6}{3\alpha_1k_2^2}-\frac{3ya_5k_2^2\alpha_1}{2\alpha_3}+a_4)^2$$
$$+(t\cdot\frac{(9\alpha_1^2k_2^4-4\alpha_2\alpha_3)a_5}{4\alpha_3}+xa_5+ya_6+a_8)^2$$
$$+k\cdot exp(-\frac{2x\alpha_3}{3\alpha_1k_2}+yk_2+\frac{(3\alpha_1^2k_2^4+4\alpha_2\alpha_3)t}{6\alpha_1k_2}+k_4) \quad (25)$$

where$a_4,a_5,a_6,a_8,k,k_2,k_4$denote arbitrary real numbers. As the denominator cannot be zero, the condition$\alpha_1\neq 0,k_2\neq 0,\alpha_3\neq 0$ must hold for Eq.(24).

Substituting Equation (25) into Equation (2), the expressions for *u* and *w* are obtained

$$u=-(2(\frac{4(\frac{ta_6(9\alpha_1^2k_2^4-4\alpha_2\alpha_3)}{6\alpha_1k_2^2}+\frac{2x\alpha_3a_6}{3\alpha_1k_2^2}-\frac{3ya_5k_2^2\alpha_1}{2\alpha_3}+a_4)\alpha_3a_6}{3\alpha_1k_2^2}+2(\frac{t(9\alpha_1^2k_2^4-4\alpha_2\alpha_3)a_5}{4\alpha_3}$$
$$+xa_5+ya_6+a_8)a_5-\frac{2k\alpha_3e^{-\frac{2x\alpha_3}{3\alpha_1k_2}+k_2y+\frac{(3\alpha_1^2k_2^4+4\alpha_2\alpha_3)}{6\alpha_1k_2}t+k_4}}{3\alpha_1k_2}))$$
$$\Big/((\frac{ta_6(9\alpha_1^2k_2^4-4\alpha_2\alpha_3)}{6\alpha_1k_2^2}+\frac{2x\alpha_3a_6}{3\alpha_1k_2^2}-\frac{3ya_5k_2^2\alpha_1}{2\alpha_3}+a_4)^2+(\frac{t(9\alpha_1^2k_2^4-4\alpha_2\alpha_3)a_5}{4\alpha_3}$$
$$+xa_5+ya_6+a_8)^2+ke^{-\frac{2x\alpha_3}{3\alpha_1k_2}+k_2y+\frac{(3\alpha_1^2k_2^4+4\alpha_2\alpha_3)}{6\alpha_1k_2}t+k_4} \quad (26)$$

The expression for *w* is similar to that for yo*u*; thus, it is not presented here. To gain a deeper understanding of the propagation properties of the solutions to the Equation, appropriate parameters are selected for discussion.

3.1. Inelastic Collision in the Form of Splitting

When the parameters take real values, the solution to Equation (1) exhibits a fission interaction, and the structure of the

solitons changes, which is characteristic of an inelastic collision. Specifically, taking the parameter$k = 1, k_2 = 2, k_4 = 2, a_4 = 1, a_5 = 2, a_6 = 3, a_8 = 4, \alpha_1 = -1, \alpha_2 = 4, \alpha_3 = 2.$, the relevant evolution diagrams are shown in Figures 20 and 21, respectively. Figure 20 illustrates the soliton solution structure of *u*. From this figure, it is evident that as time evolves, the structure of yo*u* splits from one kink soliton into one lump soliton and one kink soliton. As shown in Figure 21, the solution morphology of *w* differs from that of yo*u*, while the splitting process is analogous.

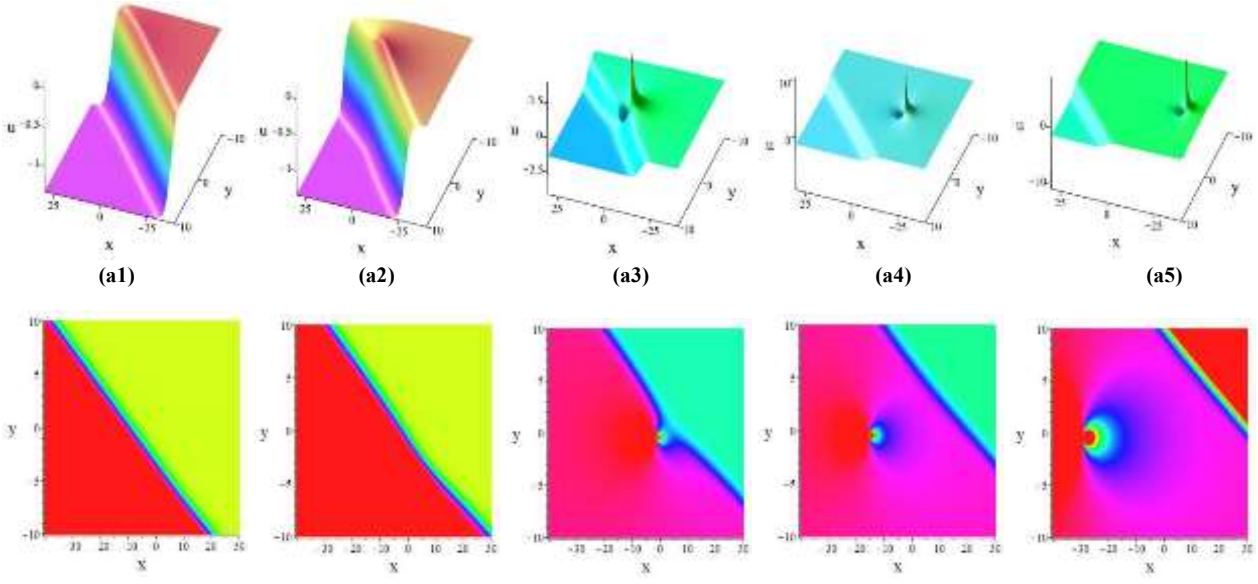

Fig. 20 The Evolution Behavior of the Mixed-Type Soliton of Equation (1) for the Component *u*. (a1) 3D Structure at *t* = -2; (a2) 3D Structure at *t* = -1; (a3) 3D Structure at *t* = 0; (a4) 3D Structure at *t* = 1; (a5) 3D Structure at *t* = 2; (b1) 2D Density Plot at *t* = -2; (b2) 2D Density Plot at *t* = -1; (b3) 2D Density Plot at *t* = 0; (b4) 2D Density Plot at *t* = 1; (b5) 2D Density Plot at *t* = 2.

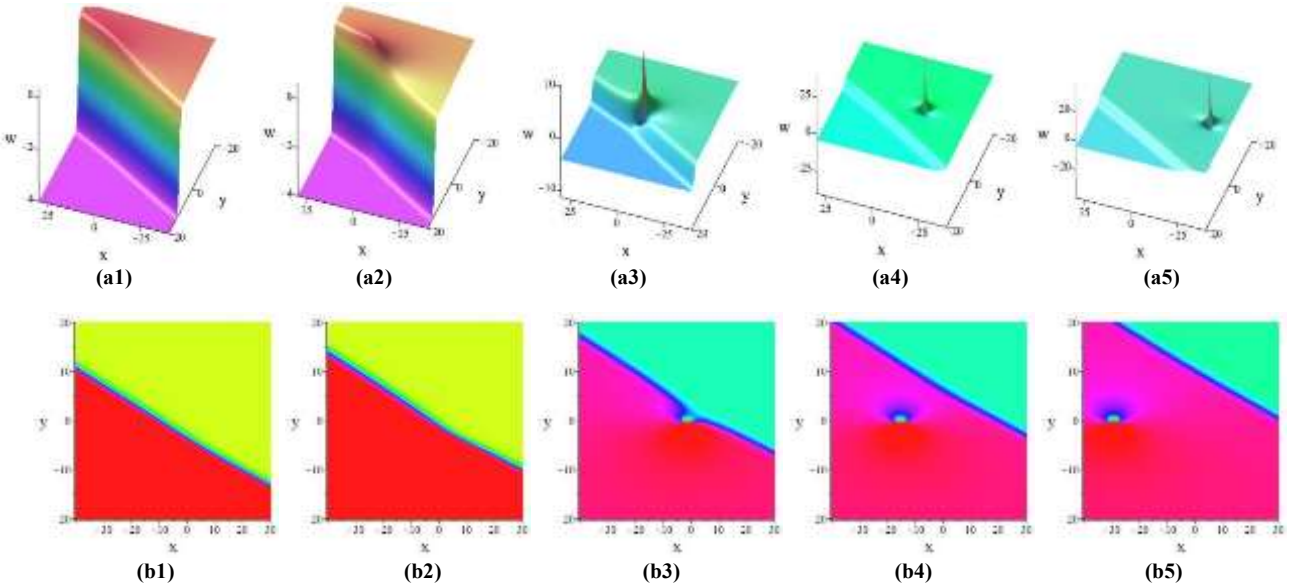

Fig. 21 The Evolution Behavior of the Mixed-Type Soliton of Equation (1) for the Component *w*. (a1) 3D Structure at *t* = -2; (a2) 3D Structure at *t* = -1; (a3) 3D Structure at *t* = 0; (a4) 3D Structure at *t* = 1; (a5) 3D Structure at *t* = 2; (b1) 2D Density Plot at *t* = -2; (b2) 2D Density Plot at *t* = -1; (b3) 2D Density Plot at *t* = 0; (b4) 2D Density Plot at *t* = 1; (b5) 2D Density Plot at *t* = 2.

3.2. Inelastic Collision in the Form of Fusion

When some of these parameters take negative real values, the solution to Equation (1) exhibits a fusion interaction—a typical characteristic of inelastic collisions. Such phenomena differ from the elastic interactions discussed in Section 2. Specifically, taking the parameters$k = 1, \quad k_2 = -1, k_4 = -1, a_4 = -1, a_5 = 2, a_6 = -3, a_8 = -4, \alpha_1 = -1, \alpha_2 = -4, \alpha_3 = -2,$, the relevant evolution diagrams are shown in Figures 22 and 23. Figure 22 illustrates the energy distribution of u. It can be observed from the figure that as time evolves, one lump soliton and one kink soliton merge into one kink soliton. The situation of *w* is similar to that of yo*u*, as presented in Figure 23.

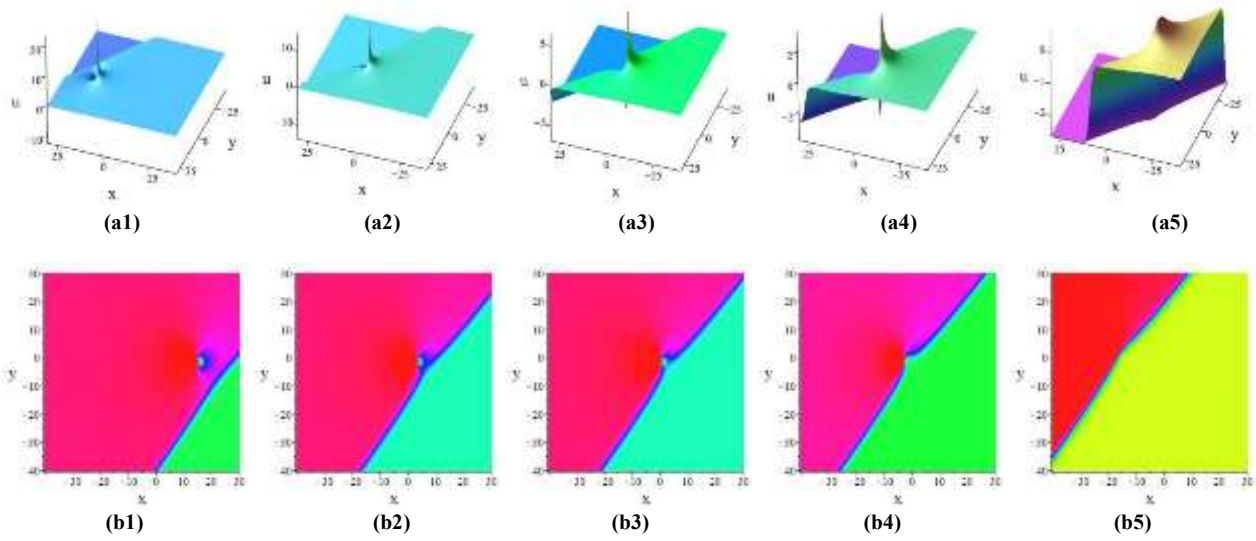

Fig. 22 The Evolution Behavior of the Mixed-Type Soliton of Equation (1) for the Component *u*. (a1) 3D Structure at *t* = -5; (a2) 3D Structure at *t* = -1; (a3) 3D Structure at *t* = 0; (a4) 3D Structure at *t* = 1; (a5) 3D Structure at *t* = 5; (b1) 2D Density Plot at *t* = -5; (b2) 2D Density Plot at *t* = -1; (b3) 2D Density Plot at *t* = 0; (b4) 2D Density Plot at *t* = 1; (b5) 2D Density Plot at *t* = 5.

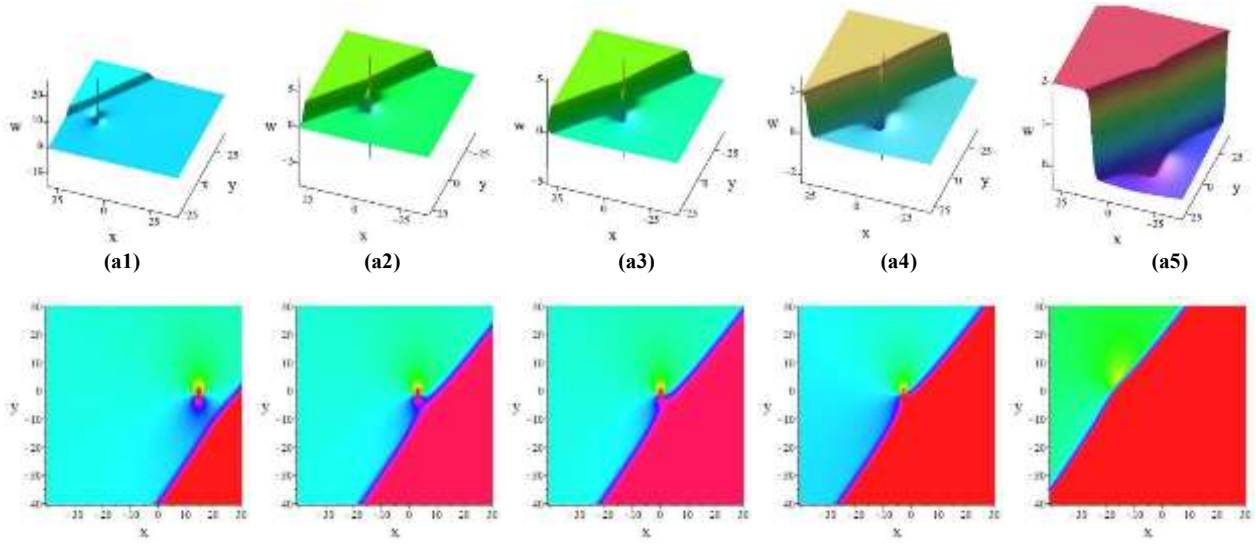

Fig. 23 The Evolution Behavior of the Mixed-Type Soliton of Equation (1) for the Component *w*. (a1) 3D Structure at *t* = -5; (a2) 3D Structure at *t* = -1; (a3) 3D Structure at *t* = 0; (a4) 3D Structure at *t* = 1; (a5) 3D Structure at *t* = 5; (b1) 2D Density Plot at *t* = -5; (b2) 2D Density Plot at *t* = -1; (b3) 2D Density Plot at *t* = 0; (b4) 2D Density Plot at *t* = 1; (b5) 2D Density Plot at *t* = 5.

4. Conclusion

In this paper, utilizing the Hirota bilinear approach, the *N*-soliton solutions and localized nonlinear interaction solutions are derived for the (2+1)-dimensional nonlinear wave equation. Through the ingenious selection of parameters, specific interaction solutions among distinct soliton types, including kink solitons, anti-kink solitons, lump solitons, and periodic solitons, are obtained. Compared with the limitation of existing studies that only focus on a single type of soliton solutions or simple interaction patterns, this paper, through the precise regulation and ingenious selection of parameters, provides a new idea for the research on solutions of integrable equations of the same type, with its parameter regulation and solution classification methods. To validate the dynamic behaviors of these solitons, a numerical simulation is conducted. Over time, graphical plots (generated via Maple) are used to exhibit various interaction phenomena between different solitons, and it is shown that there exist elastic and inelastic localized wave solitons for the studied Equation in this paper. The obtained results are novel, interesting, and also very helpful for better understanding the nonlinear phenomena of a number of wave equations in integrable systems. Future work will explore the complex interactions between nonlinear terms and higher-order dispersion terms in other nonlinear wave equations. Additionally, the applications of the obtained soliton solutions in specific physical

scenarios will be investigated, the connection between theoretical solutions and actual physical phenomena established, and new breakthroughs provided for solving practical engineering and physical problems.

Funding Statement

This research was funded by the Doctoral Fund of Henan Polytechnic University (Grant No. B2020-35) and the Fundamental Research Funds for the Universities of Henan Province (Grant No. NSFRF230430).

References

[1] J. Guo et al., "Observation of Vector Solitons Supported by Third-order Dispersion," *Physical Review A*, vol. 99, 2019. [CrossRef] [Google Scholar] [Publisher Link]

[2] Alwyn C. Scott, "Dynamics of Davydov Solitons," *Physical Review A*, vol. 26, 1982. [CrossRef] [Google Scholar] [Publisher Link]

[3] Md Nur Hossain et al., "A New Investigation of the Extended Sakovich Equation for Abundant Soliton Solution in Industrial Engineering Via Two Efficient Techniques," *Open Physics*, vol. 22, no. 1, 2024. [CrossRef] [Google Scholar] [Publisher Link]

[4] Xueming Liu, Xiankun Yao, and Yudong Cui, "Real-time Observation of the Buildup of Soliton Molecules," *Physical Review Letters*, vol. 121, 2018. [CrossRef] [Google Scholar] [Publisher Link]

[5] Sangwook Park et al., "Compact HF Surface Wave Radar Data Generating Simulator for Ship Detection and Tracking," *IEEE Geoscience and Remote Sensing Letters*, vol. 14, no. 6, pp. 969–973, 2017. [CrossRef] [Google Scholar] [Publisher Link]

[6] Mark J. Ablowitz, "Nonlinear Waves and The Inverse Scattering Transform," *Optik*, vol. 278, 2023. [CrossRef] [Google Scholar] [Publisher Link]

[7] Mark J. Ablowitz, and Ziad H. Musslimani, "Inverse Scattering Transform for the Integrable Nonlocal Nonlinear Schrödinger Equation," *Nonlinearity*, vol. 29, 2016. [CrossRef] [Google Scholar] [Publisher Link]

[8] Peng-Fei Han, Yi Zhang, and Chi-Hui Jin, "Novel Evolutionary Behaviors of Localized Wave Solutions and Bilinear Auto-Bäcklund Transformations for the Generalized (3+1)-Dimensional Kadomtsev–Petviashvili Equation," *Nonlinear Dynamics*, vol. 111, pp. 8617–8636, 2023. [CrossRef] [Google Scholar] [Publisher Link]

[9] Peng-Fei Han, and Yi Zhang, "Investigation of Shallow Water Waves Near the Coast or in Lake Environments Via the KdV–Calogero–Bogoyavlenskii–Schiff Equation," *Chaos, Solitons Fractals*, vol. 184, 2024. [CrossRef] [Google Scholar] [Publisher Link]

[10] Xi-Hu Wu, and Yi-Tian Gao, "Generalized Darboux Transformation and Solitons for the Ablowitz–Ladik Equation in an Electrical Lattice," *Applied Mathematics Letters*, vol. 137, 2023. [CrossRef] [Google Scholar] [Publisher Link]

[11] Liming Ling, Li-Chen Zhao, and Boling Guo, "Darboux Transformation and Multi-dark Soliton for N-component Nonlinear Schrödinger Equations," *Nonlinearity*, vol. 28, pp. 3243–3261, 2015. [CrossRef] [Google Scholar] [Publisher Link]

[12] Purobi Rani Kundu et al., "The Sine-Gordon Expansion Method for Higher-dimensional NLEEs and Parametric Analysis," *Heliyon*, vol. 7, no. 3, 2021. [Google Scholar] [Publisher Link]

[13] Anne Boutet de Monvel, Dmitry Shepelsky, and Lech Zielinski, "The Short Pulse Equation by a Riemann–Hilbert Approach," *Letters in Mathematical Physics*, vol. 107, pp. 1345–1373, 2017. [CrossRef] [Google Scholar] [Publisher Link]

[14] D. Kumar, K. Hosseini, and F. Samadani, "The Sine-Gordon Expansion Method to Look for the Traveling Wave Solutions of the Tzitzéica Type Equations in Nonlinear Optics," *Optik*, vol. 149, pp. 439–446, 2017. [CrossRef] [Google Scholar] [Publisher Link]

[15] H. M. Srivastava et al., "Traveling Wave Solutions to Nonlinear Directional Couplers by Modified Kudryashov Method," *Physica Scripta*, vol. 95, 2020. [CrossRef] [Google Scholar] [Publisher Link]

[16] Khalid K. Ali et al., "New Soliton Solutions of Dual Mode Sawada Kotera Equation using a New form of Modified Kudryashov Method and The Finite Difference Method," *Journal of Ocean Engineering and Science*, vol. 9, no. 3, pp. 207–215, 2024. [CrossRef] [Google Scholar] [Publisher Link]

[17] Yaqing Liu, Xiao-Yong Wen, and Deng-Shan Wang, "The N-soliton Solution and Localized Wave Interaction Solutions of the (2+1)-Dimensional Generalized Hirota-Satsuma-Ito Equation," *Computer & Mathematics with Applications*, vol. 77, no. 4, pp. 947–966, 2019. [CrossRef] [Google Scholar] [Publisher Link]

[18] Bohan Chen et al., "Lump Solution, Lump and Soliton Interaction Solution, Breather Solution, and Interference Wave Solution for the (3+1)-Dimensional Fourth-order Nonlinear Equation by Bilinear Neural Network Method," *Modern Physics Letters B*, vol. 39, no. 27, 2025. [CrossRef] [Google Scholar] [Publisher Link]

[19] Engui Fan, "An Algebraic Method for Finding a Series of Exact Solutions to Integrable and Nonintegrable Nonlinear Evolution Equations," *Journal of Physics A: Mathematical and General*, vol. 36, no. 25, 2003. [CrossRef] [Google Scholar] [Publisher Link]

[20] Juncai Pu, and Yong Chen, "Lax Pairs Informed Neural Networks Solving Integrable Systems," *Journal of Computational Physics*, vol. 510, 2024. [CrossRef] [Google Scholar] [Publisher Link]

[21] Han-Peng Chai, Bo Tian, and Zhong Du, "Localized Waves for the Mixed Coupled Hirota Equations in an Optical Fiber," *Communications in Nonlinear Science and Numerical Simulation*, vol. 70, pp. 181–192, 2019. [CrossRef] [Google Scholar] [Publisher Link]

[22] Hui Wang, "Lump and Interaction Solutions to the (2+1)-Dimensional Burgers Equation," *Applied Mathematics Letters*, vol. 85, pp. 27–34, 2018. [CrossRef] [Google Scholar] [Publisher Link]

[23] Wen-Xiu Ma, and Yuan Zhou, "Lump Solutions to Nonlinear Partial Differential Equations Via Hirota Bilinear Forms," *Journal of Differential Equations*, vol. 264, no. 4, pp. 2633–2659, 2018. [CrossRef] [Google Scholar] [Publisher Link]

[24] Bo Ren, and Ji Lin, "The Integrability of a (2+1)-Dimensional Nonlinear Wave Equation: Painlevé Property, Multi-order Breathers, Multi-order Lumps and Hybrid Solutions," *Wave Motion*, vol. 117, 2023. [CrossRef] [Google Scholar] [Publisher Link]

[25] Uttam Kumar Mandal et al., "A Generalized (2+1)-Dimensional Hirota Bilinear Equation: Integrability, Solitons and Invariant Solutions," *Nonlinear Dynamics*, vol. 111, pp. 4593–4611, 2023. [CrossRef] [Google Scholar] [Publisher Link]

[26] Zhonglong Zhao, and Lingchao He, "M-lump, High-order Breather Solutions and Interaction Dynamics of a Generalized (2+1)-Dimensional Nonlinear Wave Equation," *Nonlinear Dynamics*, vol. 100, pp. 2753–2765, 2020. [CrossRef] [Google Scholar] [Publisher Link]

[27] Xueqing Zhang, and Bo Ren, "Resonance Solitons, Soliton Molecules and Hybrid Solutions for a (2+1)-Dimensional Nonlinear Wave Equation Arising in the Shallow Water Wave," *Nonlinear Dynamics*, vol. 112, pp. 4793–4802, 2024. [CrossRef] [Google Scholar] [Publisher Link]

[28] Jian-Hong Zhuang et al., "Diverse Solitons and Interaction Solutions for the (2+1)-Dimensional CDGKS Equation," *Modern Physics Letters B*, vol. 33, no. 16, 2019. [CrossRef] [Google Scholar] [Publisher Link]